PAPER

Highly porous CO$_2$ hydrate generation aided by silica nanoparticles for potential secure storage of CO$_2$ and desalination†

Ijung Kim,[a] Michael Nole,[b] Sunghyun Jang,[b] Saebom Ko,[b] Hugh Daigle,[b] Gary A. Pope[b] and Chun Huh*[b]

We report a new way of storing CO$_2$ in a highly porous hydrate structure, stabilized by silica nanoparticles (NPs). Such a porous CO$_2$ hydrate structure was generated either by cooling down NP-stabilized CO$_2$-in-seawater foams, or by gently mixing CO$_2$ and seawater that contains silica NPs under CO$_2$ hydrate-generating conditions. With the highly porous structure, enhanced desalination was also achievable when the partial meltdown of CO$_2$ hydrate was allowed.

In situ generation of CO$_2$ hydrate at deep seabeds has been studied extensively as an economic way of sequestering anthropogenic CO$_2$,[1–3] since at the deep sea's near-freezing temperature and high hydrostatic pressure conditions, CO$_2$ hydrate can be naturally formed from a mixture of CO$_2$ and seawater.[4,5] Being solid with its density slightly higher than that of seawater, the CO$_2$ hydrate can potentially stay at the deep seabed indefinitely.[6,7] This highly attractive concept, however, has two shortcomings: first, the hydrate formation is known to occur at the interface between CO$_2$ and water and, once a hydrate layer is formed at the CO$_2$/water interface,[8] the layer serves as a barrier to further contact between CO$_2$ and water. Consequently, subsequent hydrate generation is considerably slowed down. Therefore, a vigorous mixing of CO$_2$ and water, thus a significant input of mechanical energy, is needed not only to generate as much CO$_2$/water interfacial area as possible by eliminating heat and mass transfer resistance,[9] but also to disperse the locally trapped salt that was rejected from the hydrate.[10] Second, CO$_2$ hydrate generally consists of 5.8–7.8 molecules of water per CO$_2$ molecule,[11] which means that in order to store a meaningful volume of CO$_2$ in hydrate form, an inordinate amount of water also has to be processed.

Our finding, here, is that a highly porous CO$_2$ hydrate structure can be generated by employing high internal-volume CO$_2$-in-water foam that is stabilized with hydrophilic silica nanoparticles (NPs). The concept was derived from two groups of composite materials that are based on NP-stabilized dispersions with a high internal-phase volume fraction. The first is CO$_2$-in-water foams that can be employed as an almost water-less fracturing fluid for oil and gas production;[12] the other is polymeric foams with high internal void spaces (polyHIPE), which are used as ultralight-weight, high-strength materials for a variety of chemical and biomedical applications.[13,14] The generation of both "water-less" CO$_2$ foam and polyHIPE requires the use of NPs or colloidal particles to stabilize the high internal-phase volume fraction dispersion, which has its continuous external phase in the form of very thin lamellae. In order to maintain the stability of such thin films, polymer or viscoelastic surfactant is generally needed in addition to NPs.[15] In our case, the CO$_2$ hydrate particulates generated next to NPs (that straddle the CO$_2$/water interface; see Fig. 1) appear to provide certain structural rigidity for the lamella's integrity. This is in a sense similar to polyHIPE in which, once dispersion is formed, thin lamellae polymerize and solidify, thereby generating a high-porosity, low-permeability, sturdy structure. Earlier studies[16–18] found that, when a water-in-CO$_2$ dispersion
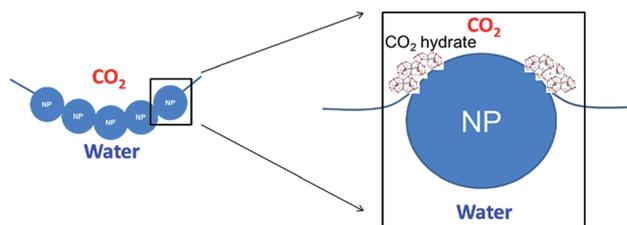
aDepartment of Civil and Environmental Engineering, Western New England University, 1215 Wilbraham Rd., Springfield, MA 01119, USA. E-mail: ijung.kim@wne.edu

bDepartment of Petroleum and Geosystems Engineering, The University of Texas at Austin, 200 E. Dean Keeton St., Stop C0300, Austin, TX 78712, USA. E-mail: chunhuh@mail.utexas.edu

† Electronic supplementary information (ESI) available: Detailed microscopic analysis, CO$_2$ hydrate generation with DI water and dry water, temperature, CO$_2$ equilibrium curve, and ion removal efficiency data. See DOI: 10.1039/c6ra26366f

Fig. 1 The presence of hydrophilic nanoparticles at the CO$_2$–water interface increases the length of the three-phase contact line, improving CO$_2$ hydrate nucleation.

is generated by way of "dry water" (water-in-air Pickering dispersion, stabilized with hydrophobic silica NPs[19]) and is subsequently brought to the hydrate-generating condition, hydrate generation kinetics are significantly enhanced. Such enhancement is in line with earlier observations that the presence of silica surface enhances CO_2 hydrate nucleation and growth. Importantly, the enhancement may result not only from the large solid surface area available from silica NPs, but also from the generation of tremendous lengths of three-phase (CO_2/water/silica) contact line on the NPs adsorbed at the CO_2/water interfaces of the dispersion. Recent molecular dynamics simulations[20] showed that the CO_2/water/silica contact line zone serves as a highly favourable nucleation site for CO_2 hydrates. Since the hydrophilic NPs stabilizes CO_2-in-water dispersions while hydrophobic NPs stabilize water-in-CO_2 dispersion, and since the use of hydrophilic NPs such as zinc oxide[21] and graphite[22] to enhance CO_2 hydrate generation has been reported, we experimentally investigated the effect of the hydrophilic silica NPs on the CO_2 hydrate generation and its structure. In addition to much lower cost of manufacturing, the hydrophilic silica NP can be easily dispersed in the water, without going through somewhat tedious step of "dry water" generation. Two important requirements for the hydrophilic NP's surface property are: (i) the NPs should have long-term dispersion stability in seawater; and (ii) they should have the hydrophilicity to form stable CO_2-in-water foams when sufficient mechanical energy input is applied. These requirements were verified for the NPs we used, based on our earlier studies.[23,24]

CO_2 hydrate formation experiments

CO_2 hydrate was generated in two different ways: (i) *via* prior generation of CO_2-in-seawater foam and (ii) by gentle mixing of CO_2 and seawater. Similar tests were conducted with DI water, also, CO_2 hydrate was generated *via* "dry water" (hydrophobic nanoparticle-stabilized water dispersion in air) as a supplementary study (details in ESI†).

The synthetic seawater (ASTM D 1141, Ricca Chemical Company®, USA) and the liquid CO_2 (Praxair, USA) were employed to generate CO_2 hydrate in the 12.5 mL sapphire cell (Separex, France). For nanoparticles, the nominal 5 nm-spherical hydrophilic silica nanoparticles coated with polyethylene glycol (3M, USA) were used.

For the CO_2 hydrate *via* CO_2-in-seawater foams, the nanoparticle-stabilized CO_2 foam generating system in previous study[25] was utilized as shown in Fig. 2(A). The CO_2 and seawater with 1 wt% hydrophilic nanoparticles were co-injected into a sandpack (filled with 350 μm Ottawa sand) by HPLC pump (1500 HPLC, Supercritical Fluid Technologies, Inc., USA) and high pressure syringe pump (500D, Teledyne ISCO, Inc., USA), generating CO_2-in-seawater foams through the effluent line at the ambient temperature. The total flow rate was controlled at 10 mL min^{-1} with a constant volume fraction of CO_2 at 0.75. At the flow condition, the interstitial velocity, shear rate, and residence time were 3.39 cm s^{-1}, 10 600 s^{-1}, and 9 s, respectively. The entire system pressure was maintained at 11.7 MPa
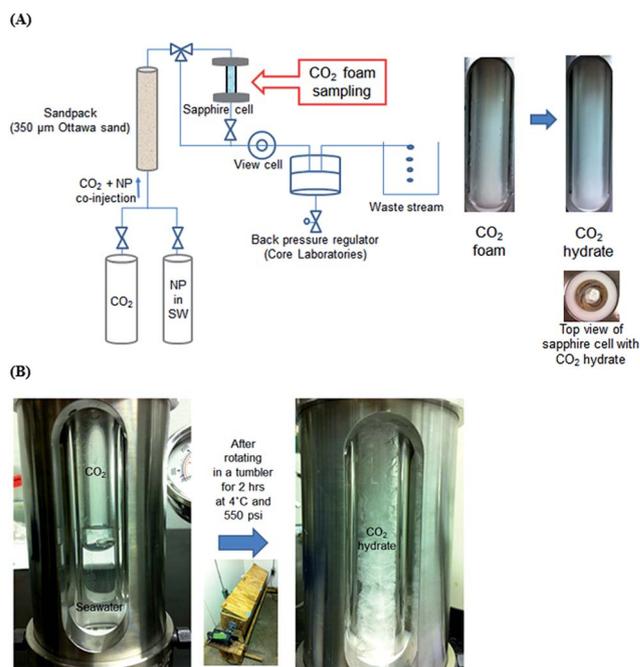

Fig. 2 Experimental system to generate CO_2 hydrate *via* (A) CO_2-in-seawater foam and (B) gentle mixing of CO_2 and seawater.

by the back pressure regulator (Core Laboratories, USA). The pressure was also monitored by the pressure gauge (Swagelok, USA) connected to the sapphire cell. When the CO_2-in-seawater foam fully filled the sapphire cell, it was then kept at 4 °C in a stationary condition for 24 h (Fig S3†).

For the hydrate formation by gentle mixing of CO_2 and seawater, the entire set-up was placed in the 4 °C cold room overnight prior to the test. The sapphire cell was filled with 6 mL of seawater with or without 1 wt% hydrophilic nanoparticles, followed by the pressurization with CO_2 up to 3.8 MPa. CO_2 was stored in a pressure vessel which was held at 3.8 MPa at 4 °C and connected to the sapphire cell to pressurize it. Once the cell was pressurized, the initial test pressure was confirmed by the pressure gauge (Kodiak Controls Inc., USA) attached to the cell. Then, the sapphire cell was placed in a tumbler which rotated at 7 rpm for 2 h. The rotating speed of the tumbler was selected to keep the CO_2 hydrate generation in a gentle mixing condition.

Overall, the following improvements in experimental procedure over the earlier reported[16–18] were made. First, the entire generation process was carried out in a 4 °C cold room to ensure a constant temperature condition. The cold room was designed to keep 4 °C constantly with a real-time temperature monitoring panel. Second, sapphire cells with pressure control were employed to directly observe the progress of hydrate generation process. After the visual observation that the hydrate generation was established, the cell was depressurized, the generated hydrate was drained of any excess water and was immediately taken in an ice bath to the cold-stage scanning electron microscopy (SEM) to obtain microscopic structural images (details in ESI†).

Note that water used in our main experiments reported here was synthetic seawater. Although the water that forms hydrate

cage does not include any salts, seawater with high salt content can still be included in between hydrate aggregates during the process of the rapid CO_2 hydrate generation.[26] Therefore, the Na^+, Mg^{2+}, and Ca^{2+} ion concentrations of the hydrate samples taken from the depressurized cell were measured by ion chromatography (Dionex ICS-1100, Thermo Scientific, USA) equipped with cation exchange column (IonPac CS12A, Thermo Scientific, USA) to quantify their change from the pre-hydrate concentrations, in order to approximately estimate the extent of seawater trapping. To further analyze the effect of CO_2 hydrate melting on the trapped ion concentrations, a part of CO_2 hydrate taken out of the sapphire cell was sampled for the ion concentration analysis before melting, and the rest of the hydrate was placed on a disposable wiper (Kimwipes, Kimberly-Clark, USA) to drain the trapped seawater for 10 min at 4 °C and ambient pressure condition, as the hydrate partially melted slowly. During the partial melting process,[27] the CO_2 hydrate was sampled at 5 and 10 min, respectively, which was allowed to melt completely for the ion chromatography analysis.

SEM observations of different hydrate structures

Fig. 3(A) shows the hydrate generated from the pre-formed CO_2-in-seawater foam stabilized with hydrophilic silica NPs. As described above, the lamella's stability was maintained by the NPs adsorbed on its two interfaces, and the newly generated hydrates attached to the NPs appear to provide additional rigidity to the lamellae. With the sapphire cell depressurization, the CO_2 bubbles would have expanded and burst the lamellae; however, unlike the conventional foam lamellae which, when destabilized, would immediately contract and disappear, the CO_2 hydrate-covered lamellae still left a considerable degree of "skeletal boundaries", similar to the polymerized polyHIPE structure. This suggests that, as discussed above with the molecular dynamics simulations,[20] the CO_2 hydrate generation from CO_2 foam occurred at three-phase contact line throughout the lamellae, forming a highly porous NP-stabilized CO_2 hydrate structure even after depressurization.

Fig. 3(B) shows a SEM image of the hydrate generated from gentle mixing of CO_2 and hydrophilic silica NP-containing seawater in a tumbler. At ambient conditions, such a gentle mixing cannot produce stable CO_2-in-water foam, because the adsorption of NPs to the CO_2/water interface requires to overcome a certain energy barrier.[28] Brought to the hydrate-generating condition, however, it appears that the CO_2-in-seawater foam generation was possible even with only moderate energy input, from synergy between the newly generated hydrate at the CO_2/water interface and the NPs that were attached to the hydrates and thus more easily brought to the CO_2/water interface. The adsorbed NPs, in turn, would enhance further hydrate generation at three-phase contact lines. The image suggests that the lamellae did not have as much rigidity as the case of pre-generated foam (Fig. 3(A)), with fewer "skeletal boundaries" remaining after the depressurization. This is probably because not as many NPs were able to be
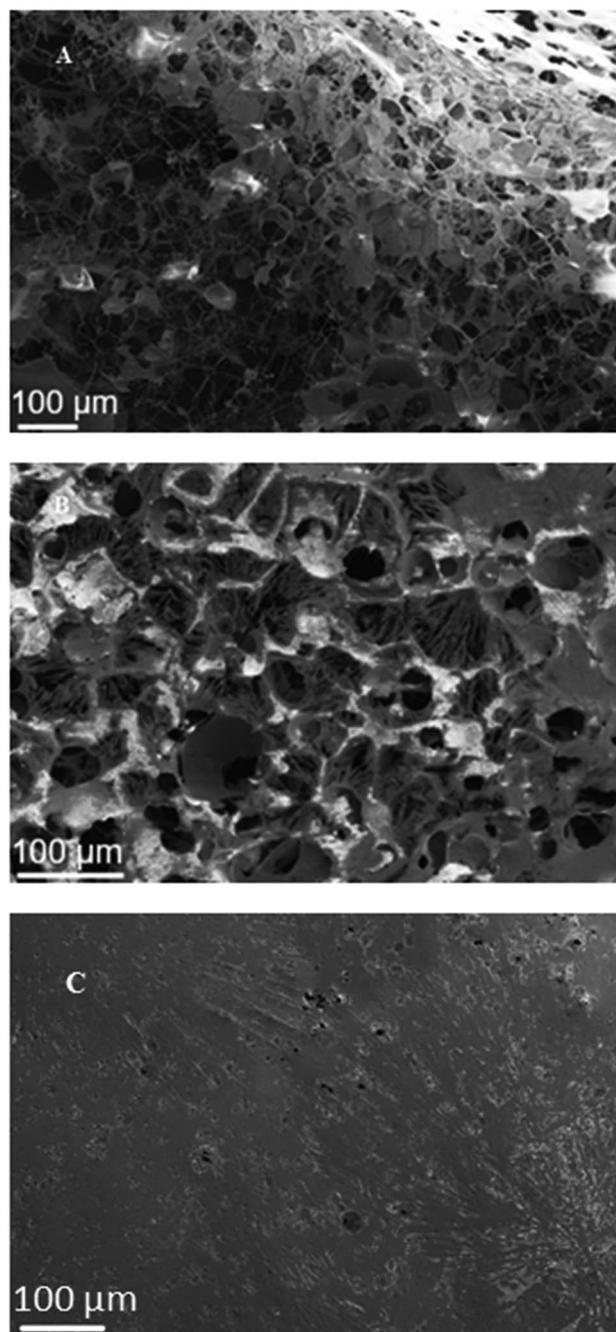

Fig. 3 SEM images of CO_2 hydrate *via* (A) nanoparticle-stabilized CO_2-in-seawater foams, (B) gentle mixing of CO_2 and seawater with nanoparticles, and (C) gentle mixing of CO_2 and seawater without nanoparticles.

adsorbed at the bubble interface, due to insufficient mixing energy input. Also the larger pore size suggests larger CO_2 bubbles. Nevertheless, it seems that the NP-stabilized CO_2 hydrate structure, even generated with gentle mixing only, could hold a substantial volume of CO_2 throughout the numerous lamellae. The NPs added to water thus appear to contribute to formation of a highly porous CO_2 hydrate structure by way of generation of CO_2 foams with highly stable, NP-stabilized lamellae.

Fig. 3(C) shows the CO_2 hydrate generated from gentle mixing of CO_2 and seawater, but without NPs. The planar surface indicates that there was little possibility to form stable CO_2 bubbles without the NPs. As a result, the CO_2/seawater interface as a large plane served as the CO_2 hydrate generation sites, leading to a planar growth in the entire cell. This type of surface structure was also found with the CO_2 hydrate generated by gentle mixing of CO_2 and DI water (Fig. S1(A)†). This also suggests that the stability of the CO_2 hydrate-induced CO_2/seawater dispersion in the absence of NPs is rather tenuous, and the ability of such hydrate structure to hold CO_2 is quite uncertain.

Fig. 4 shows a nanoscale SEM image of CO_2 hydrate generated by gentle mixing of CO_2 and seawater with NPs (see Fig. 3(B)). The skeletal structure, which is the vestige of the CO_2 foam lamellae, was clearly captured, displaying its thickness around 200–500 nm. The swollen three-way junction appears to represent a plateau border with the formerly continuous aqueous phase.[29] This SEM image suggests simultaneous CO_2 foam generation and hydrate generation. Although the threshold shear rate is required to overcome the adsorption energy barrier[24] for CO_2 foam generation, little has been studied for the CO_2 foam generation at such a low temperature. The CO_2 foam stability was known to increase as temperature decreases. Also, the increased CO_2 density at such a low temperature would require less mechanical mixing for CO_2 foam generation.[23] In addition, the nucleation and the growth of CO_2 hydrate in the CO_2/seawater mixture might provide additional shear to the fluid as small solid CO_2 hydrate particles or aggregates rotate in it.

Salinities in different hydrate structures

In principle, CO_2 hydrate generation can be a good desalination method because hydrate molecular cage contains water with zero salinity. However, when CO_2 hydrate is generated from seawater, the seawater inclusion among CO_2 hydrate aggregates is inevitable, leaving a certain level of salinity. Since the highly porous CO_2 hydrate would trap less seawater due to their more internally connected structure, it was desirable to measure the salinity from the CO_2 hydrate samples. Because it is difficult to distinguish the hydrate from the trapped seawater based on the SEM images of the skeletal structure, the following indirect way
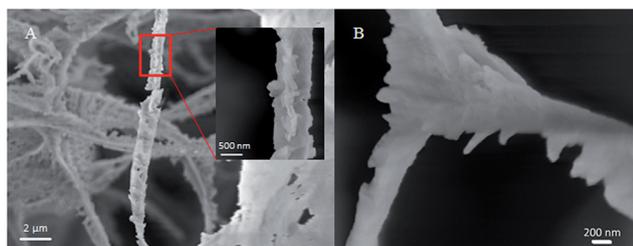
of estimating the respective mass fractions of major salt ions was attempted. After the CO_2 hydrate samples were taken out from the depressurized sapphire cell and excess seawater was drained off, three different samples were prepared; one taken immediately after the seawater drainage; and two taken after 5 and 10 minutes of the partial melting of CO_2 hydrate sample at 4 °C for the further drainage and removal of the trapped seawater. Then, the concentration of three major cations (Na^+, Mg^{2+}, and Ca^{2+} ion initially 1.13%, 0.06%, and 0.13%, respectively) in seawater was measured from these three different samples. Fig. 5 shows the overall removal efficiency (measured concentration over original seawater concentration) of the salt ions. Without partial melting, the removal efficiency was 6.68–9.24% higher with NPs than without NPs. When the samples were taken after the partial melting was allowed for 10 min, the
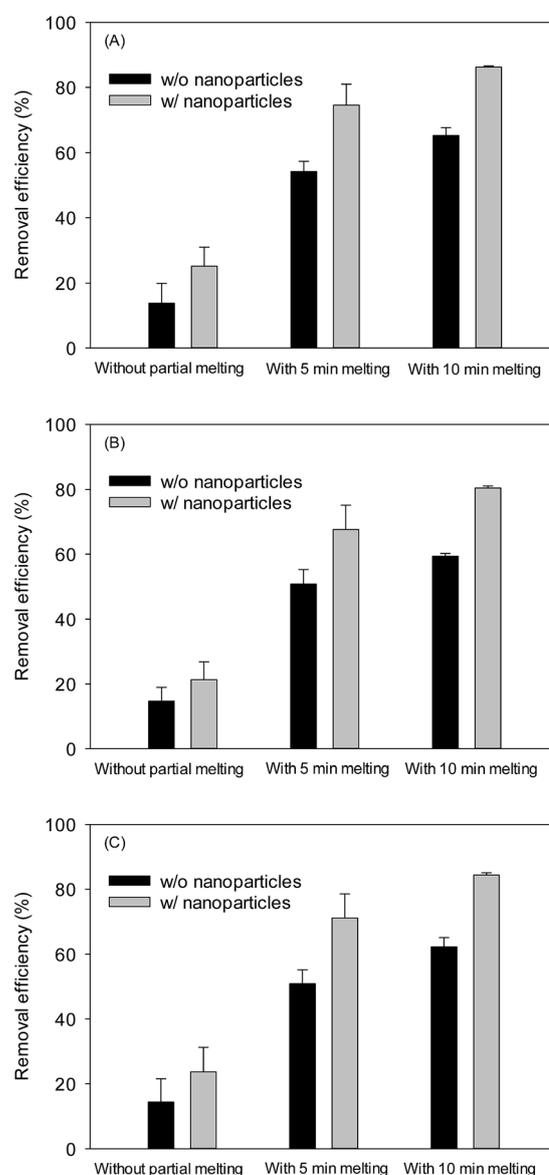

Fig. 4 Nanoscale SEM image of CO_2 hydrate formed by gentle mixing of CO_2 and seawater with nanoparticles: focusing on (A) a rod and (B) a three-way junction.

Fig. 5 Effect of nanoparticles on removal efficiency of major cations in seawater *via* CO_2 hydrate followed by a partial melting: (A) Na^+, (B) Mg^{2+}, and (C) Ca^{2+}.

removal efficiency was increased up to 65.30% (without NPs) and 86.26% (with NPs), supporting the greater drainage rate of the trapped seawater with NPs, specifically, with the highly porous structure. The ESI data regarding the removal efficiency is included in Table S1.† The qualitatively similar removal trend was obtained over the series of tests although some fluctuations in the measurements were also observed because the identical CO_2 hydrate surface area was difficult to obtain. Therefore, the constant test condition with a detailed control protocol should be maintained to minimize the fluctuations in the removal efficiency. Considering the similar trend in removal pattern among the major ions tested here, other minor salts are expected to show such removal pattern as well. In fact, for the hydrate-based desalination process,[30] the salt trapping turned out to be a major hindrance for its practical development. The facts that the NP-aided CO_2 hydrate structure contained much less trapped salt, and that the drainage of trapped seawater was achievable by simple partial melting of CO_2 hydrate, offer an intriguing possibility that NP-aided CO_2 hydrate-based desalination process may provide an economic way of producing low-salinity water, *e.g.*, for the recently developed low-salinity enhanced oil recovery process for offshore oilfields.[31]

Conclusions

Based on the CO_2 hydrate formation mechanism, it is expected that the diffusion of water to liquid CO_2 would occur along with the hydrophilic silica NP surface located at the CO_2/water interface, offering numerous sites for CO_2 hydrate nucleation. In addition, the conversion of CO_2-in-seawater foams to CO_2 hydrate shown in this study demonstrates the CO_2 hydrate could be pre-shaped in a lamellar structure resulting in a highly porous CO_2 hydrate.

The generation of such highly porous CO_2 hydrate structure, *in situ* either in geological formations or at subsea, has a couple of potential applications. First, such porous hydrate structures containing CO_2 could be securely sequestered in quantity in the shallow subsurface of deep-sea sediments, which are abundantly available worldwide. Second, as described above, an economic desalination process could be developed *via* natural formation of NP-stabilized CO_2 hydrate, at subsea, to obtain low-salinity water for injection for enhanced oil recovery from offshore oil reservoirs. The currently available desalination options are either too costly or difficult to implement on platforms. Such utilization of CO_2 in hydrate form will improve the overall economics of CO_2 sequestration as well as offshore oilfield operation, so that CO_2 can be sequestered in truly meaningful quantities.

Acknowledgements

References

1 P. Linga, R. Kumar and P. Englezos, *J. Hazard. Mater.*, 2007, **149**, 625–629.

2 H. Tajima, A. Yamasaki, F. Kiyono and H. Teng, *AIChE J.*, 2004, **50**, 871–878.

3 B. Tohidi, J. H. Yang, M. Salehabadi, R. Anderson and A. Chapoy, *Environ. Sci. Technol.*, 2010, **44**, 1509–1514.

4 K. Z. House, D. P. Schrag, C. F. Harvey and K. S. Lackner, *Proc. Natl. Acad. Sci. U. S. A.*, 2006, **103**, 12291–12295.

5 K. Ohgaki, Y. Makihara and K. Takano, *J. Chem. Eng. Jpn.*, 1993, **26**, 558–564.

6 S. Lee, L. Liang, D. Riestenberg, O. R. West, C. Tsouris and E. Adams, *Environ. Sci. Technol.*, 2003, **37**, 3701–3708.

7 D. E. Riestenberg, C. Tsouris, P. G. Brewer, E. T. Peltzer, P. Walz, A. C. Chow and E. E. Adams, *Environ. Sci. Technol.*, 2005, **39**, 7287–7293.

8 F. Lehmkuhler, M. Paulus, C. Sternemann, D. Lietz, F. Venturini, C. Gutt and M. Tolan, *J. Am. Chem. Soc.*, 2009, **131**, 585–589.

9 M. A. Clarke and P. R. Bishnoi, *Chem. Eng. Sci.*, 2005, **60**, 695–709.

10 C. Tsouris, P. Szymcek, P. Taboada-Serrano, S. McCallum, P. Brewer, E. Peltzer, P. Walz, E. Adams, A. Chow and W. Johnson, *Energy Fuels*, 2007, **21**, 3300–3309.

11 D. Kyung, H.-K. Lim, H. Kim and W. Lee, *Environ. Sci. Technol.*, 2015, **49**, 1197–1205.

12 Z. Xue, A. J. Worthen, C. Da, A. Qajar, I. R. Ketchum, S. Alzobaidi, C. Huh, M. Prodanovic and K. P. Johnston, *Langmuir*, 2015, **32**, 28–37.

13 I. Pulko, M. Kolar and P. Krajnc, *Sci. Total Environ.*, 2007, **386**, 114–123.

14 C. Zhao, E. Danish, N. R. Cameron and R. Kataky, *J. Mater. Chem.*, 2007, **17**, 2446–2453.

15 S. Siripurapu, J. M. DeSimone, S. A. Khan and R. J. Spontak, *Macromolecules*, 2005, **38**, 2271–2280.

16 B. O. Carter, W. Wang, D. J. Adams and A. I. Cooper, *Langmuir*, 2009, **26**, 3186–3193.

17 F. Farhang, A. V. Nguyen and M. A. Hampton, *Energy Fuels*, 2014, **28**, 1220–1229.

18 F. Farhang, A. V. Nguyen and K. B. Sewell, *Energy Fuels*, 2014, **28**, 7025–7037.

19 B. P. Binks and R. Murakami, *Nat. Mater.*, 2006, **5**, 865–869.

20 D. Bai, G. Chen, X. Zhang and W. Wang, *Langmuir*, 2012, **28**, 7730–7736.

21 M. Mohammadi, A. Haghtalab and Z. Fakhroueian, *J. Chem. Thermodyn.*, 2016, **96**, 24–33.

22 S.-d. Zhou, Y.-s. Yu, M.-m. Zhao, S.-l. Wang and G.-z. Zhang, *Energy Fuels*, 2014, **28**, 4694–4698.

23 A. J. Worthen, H. G. Bagaria, Y. Chen, S. L. Bryant, C. Huh and K. P. Johnston, *J. Colloid Interface Sci.*, 2013, **391**, 142–151.

24 T. Zhang, M. J. Murphy, H. Yu, H. G. Bagaria, K. Y. Yoon, B. M. Nielson, C. W. Bielawski, K. P. Johnston, C. Huh and S. L. Bryant, *SPE J.*, 2014, **20**, 667–677.

25 I. Kim, A. J. Worthen, K. P. Johnston, D. A. DiCarlo and C. Huh, *J. Nanopart. Res.*, 2016, **18**, 82–93.

26 A. P. Camps, Hydrate formation in near surface ocean sediments, PhD thesis, University of Leicester, 2008.

27 W. Gu, Y.-B. Lin, Y.-J. Xu, W.-B. Chen, J. Tao and S. Yuan, *Cold Reg. Sci. Technol.*, 2013, **86**, 133–141.

28 B. P. Binks and T. S. Horozov, *Colloidal particles at liquid interfaces*, Cambridge University Press, 2006.

29 C. J. W. Breward and P. D. Howell, *J. Fluid Mech.*, 2002, **458**, 379–406.

30 K. Park, S. Y. Hong, J. W. Lee, K. C. Kang, Y. C. Lee, M.-G. Ha and J. D. Lee, *Desalination*, 2011, **274**, 91–96.

31 N. Morrow and J. Buckley, *J. Pet. Technol.*, 2011, **63**, 106–112.